FREQUENCY-MODULATED AND SINGLE-TONE EXCITATION TO REVEAL VIBRO-ACOUSTIC NONLINEARITIES IN LOOSENED BOLTED JOINTS

Berkay Kullukcu[1], Robin Pianowski[1], Dina Hannebauer[1]

[1] *FG Maschinendynamik und Akustik, Technische Hochschule Wildau, 15745 Brandenburg, Germany*

This paper is a revised version of the authors' submitted manuscript that was peer-reviewed by at least two anonymous reviewers.

Abstract

Preload loss in bolted joints alters structural stiffness, damping, and nonlinearity. This paper evaluates a shaker-based vibro-acoustic method on a rail-vehicle-inspired beam assembly. The central M10 fastener (S2) in a three-bolt lap joint between two steel beams, representing bolted interfaces on carbody and roof-mounted components, was tested at 0%, 20%, 40%, and 80% preload. A triaxial accelerometer measured the structural response, while a microphone placed 300 mm from S2 recorded the radiated sound as a secondary sensing channel. Sine-sweep and narrow-band excitation identified a dominant resonance near 130 Hz. Under 130 Hz single-tone excitation, the loose state produced additional high-frequency spectral components in the accelerometer response. Frequency-modulated (FM) excitation from 125 to 135 Hz further separated the preload states through harmonic-band levels relative to the carrier: the loose-to-80% differences were 17.5 dB in the second-harmonic band and 36.5 dB in the sixth-harmonic band.

Keywords: *bolt loosening detection, preload loss, rail vehicle structures, frequency-modulated excitation*

1. Introduction

Bolted joints are widely used because of their high load capacity, demountability, and low cost. Their function depends on an adequate clamp force that keeps the connected parts in frictional contact [1]–[3]. A reduction in preload changes the effective stiffness and damping of the interface and can initiate rattle, fatigue accumulation, and safety-relevant degradation under repeated vibration and shock [2], [3]. Thus, a highly preloaded joint behaves approximately as a stiff, frictionally damped connection, whereas a loose joint behaves as a softer contact with stronger and less predictable nonlinearity [2].

Figure 1: Couplings between train wagons include many different types of bolted connections which get loosened after continous vibration.

Rail vehicles, as also shown in Fig. 1, contain bolted interfaces in the carbody, roof-mounted equipment, bogie-related assemblies, and fastening systems. These interfaces experience broadband and transient excitation caused by track irregularities, wheel–rail interaction, curving, braking, and traction [5]–[8]. A portable shaker combined with a small number of response sensors can therefore be useful during scheduled maintenance at accessible carbody or roof locations [20]–[22]. This approach is not equally practical at every location: restricted space and access, particularly near the bogie, may require a compact exciter, an impact source, or the use of operational excitation instead of the shaker configuration used here.

Transverse excitation can produce micro-slip and macro-slip at a bolted interface. Once the transverse motion overcomes thread and bearing-surface friction, incremental bolt rotation and preload loss can occur, as demonstrated by the Junker transverse-vibration configuration [2], [4]. In a lap joint, repeated transitions between sticking and slipping can therefore produce both self-loosening and nonlinear dynamic response [9], [10].

DIN 65151 and ISO 16130 standardize transverse-vibration tests for comparing clamp-force decay under

Corresponding author: *berkay.kullukcu@th-wildau.de.*

controlled displacement excitation [9], [11]. Such tests require access to axial force or preload, which is often unavailable on an existing vehicle. Instrumented bolts and piezoelectric transducers can provide high sensitivity [19], but replacing every relevant fastener with a sensing element is generally impractical. In contrast, accelerometers can be attached externally and microphones can be positioned without modifying the joint.

Preload affects the interface through changes in effective stiffness, frictional energy dissipation, and nonlinearity. Micro-slip is a major source of damping in jointed structures [12]–[18]. As preload decreases, the contact can transition from sticking to partial slip and intermittent separation, causing resonance shifts, peak broadening, harmonics, sidebands, and broadband response components [12], [15], [18].

Existing bolt-monitoring studies have employed strain-sensing bolts, ultrasonic time-of-flight, electromechanical impedance, piezoelectric wave propagation, modal features, and machine-learning classifiers [19], [23]–[26]. Sound-based methods have also detected loosening from percussion or vibration-driven radiation using engineered features and classification models [27]–[34]. The acoustic field may be viewed as a radiated consequence of structural vibration, but its sensitivity also depends on radiation efficiency, microphone position, and environmental noise.

Modal testing provides a direct framework for tracking changes in resonance frequency, damping, and frequency-response shape [20]–[22]. Even sparse accelerometer measurements have been used to classify bolt-tightness states [23], [24], while natural-frequency and spectral-kurtosis measures have been proposed as interpretable indicators [25], [26].

Contact acoustic nonlinearity and vibro-acoustic modulation exploit the fact that a slipping or intermittently contacting interface acts as a nonlinear modulator. Higher-order harmonics and sidebands generally increase as the joint departs from a highly preloaded, approximately linear state [35]–[38]. Although many implementations use separate low- and high-frequency inputs, related energy-transfer effects can also be examined using a shaker in the audio-frequency range.

Current transverse-vibration standards principally quantify clamp-force reduction [9], [11], whereas many structural-health-monitoring studies focus on classification for a fixed excitation or on dedicated transducers [19], [23], [27]. Fewer studies combine controlled single-tone and FM shaker excitation, simultaneous vibration and sound measurements, and interpretable response-side nonlinear measures without direct preload sensing [35]–[37]. The present work therefore investigates excitation regimes that reveal loosening and evaluates a minimal-sensor procedure for a rail-vehicle-inspired joint.

2. Method

The demonstrator is shown in Fig. 2. An electrodynamic shaker (TMS K2007E01) introduced vibration through a plastic stinger connected to a force/acceleration sensor (PCB 288D01). A triaxial accelerometer (PCB 356A01/NC) measured the structural response on the beam. A microphone was positioned 300 mm from bolt S2 to record radiated sound simultaneously. In the present analysis, the microphone was used to verify whether the structurally identified resonance was also observable acoustically and to assess the feasibility of a non-contact secondary channel; the reported quantitative loosening metrics were calculated from the accelerometer z-axis.

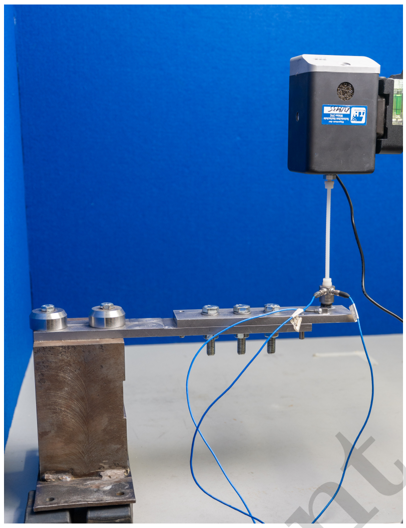

Figure 2: Rail-inspired bolted demonstrator excited by an electrodynamic shaker through a force sensor. The triaxial accelerometer measures structural response, and the microphone is positioned 300 mm from bolt S2.

The test joint consisted of three M10 bolts connecting two overlapping steel beams with nuts and washers on both sides. The central bolt S2 was the bolt under test; S1 and S3 remained at 80% preload throughout the experiment (Fig. 3). S2 was tested at nominal preload levels of 0%, 20%, 40%, and 80%, corresponding to tightening torques of 0, 12.5, 25, and 50 Nm. Two M8 bolts connecting the cantilever beams to the support block remained at 80% preload (25 Nm). For each S2 preload state, the shaker applied single-tone and FM excitation. The FM conditions used for the harmonic-band analysis were repeated three times.

The configuration represents an accessible lap-joint-type connection such as a carbody or roof-mounted equipment interface. It is not intended to reproduce the geometry or boundary conditions of a specific vehicle joint; rather, it provides a controlled platform for testing response-based indicators before transfer to more constrained locations.

3. Results

The bolt under test was first tightened to the 80% reference preload. Sine-sweep (Fig. 4) and narrow-band white-noise (Fig. 5) inputs were then applied separately to characterize the demonstrator.

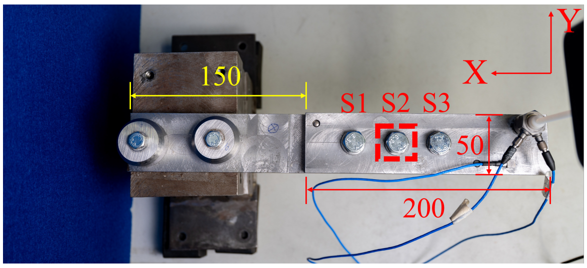

Figure 3: Demonstrator geometry and bolt positions; all dimensions are in mm and the beam thickness is 9 mm. The red dashed square identifies the central M10 bolt S2, whose preload was varied. S1 and S3 remained at 80% preload.

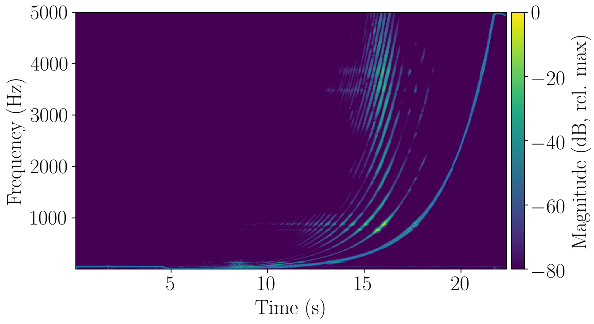

Figure 4: Sine-sweep input measured by the PCB 288D01 force/acceleration sensor.

The sine sweep covered 1–5000 Hz, while the narrow-band input covered 100–350 Hz. The response spectra are shown in Figs. 6 and 7. Both excitation types produced a dominant structural response at 130 ± 2 Hz, and the microphone trace showed that this region was also radiated acoustically. Additional resonances are visible in Fig. 6; they were not ignored, but 130 Hz was selected because it was the strongest response consistently present in both the broad sine sweep and the controlled narrow-band test and could therefore be targeted reproducibly by both single-tone and FM excitation.

A 130 Hz sinusoidal input was subsequently applied. Relative to the 50 Nm state, the loose state exhibited a raised broadband response and multiple additional or strongly amplified high-frequency spectral components in the accelerometer z-axis (Fig. 8). The five highlighted components at 1599.5, 3314.8, 3919.0, 5698.9, and 8451.1 Hz were selected as local maxima with at least 3 dB prominence and at least 80 Hz spacing. Other visible peaks or shoulders did not meet these selection criteria, were not sufficiently separated from neighbouring components, or were also present in the tight-state spectrum; they were therefore not used as discrete indicators.

The FM excitation was generated as

$$x(t) = A \sin(2\pi f_c t + \beta \sin(2\pi f_m t)), \quad (1)$$

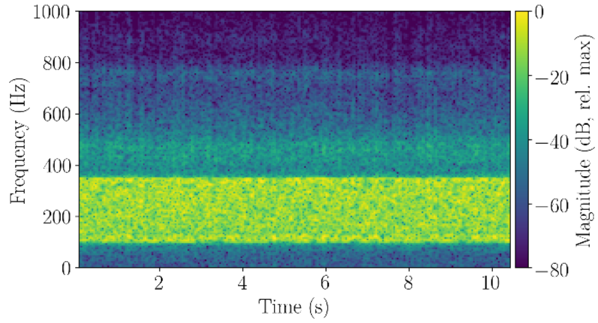

Figure 5: Narrow-band white-noise input measured by the PCB 288D01 force/acceleration sensor.

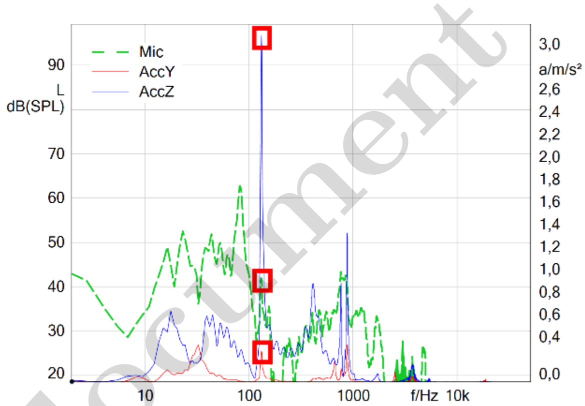

Figure 6: Measured response under sine-sweep excitation. Several resonances are visible; the response near 130 Hz was selected for the controlled tests because it was prominent in both the accelerometer and microphone channels and was reproduced by the narrow-band excitation.

where A is the excitation amplitude, f_c is the carrier frequency, f_m is the modulation frequency, and β is the modulation index. The instantaneous frequency is

$$f_i(t) = f_c + \beta f_m \cos(2\pi f_m t). \quad (2)$$

For all tests, $f_c = 130$ Hz and the peak frequency deviation was $\Delta f = 5$ Hz; therefore, $\beta = \Delta f / f_m$ was adjusted so that the instantaneous frequency always spanned 125–135 Hz. The tested modulation frequencies were 1, 2, 5, 10, and 20 Hz.

The clearest separation among the examined FM conditions was obtained for $f_m = 2$ Hz. The harmonic-band level relative to the carrier was calculated as

$$R_l = 10 \log_{10} \left(\frac{P_{\text{out}}(l)}{P_{\text{out}}(130\,\text{Hz})} \right), \quad (3)$$

where $P_{\text{out}}(130\,\text{Hz})$ is the output power in the carrier band and $P_{\text{out}}(l)$ is the output power in the l-th harmonic band. Negative values therefore indicate that the harmonic-band power is below the carrier-band power; a less negative value represents a stronger harmonic relative to the carrier. For the 125–135 Hz FM input, the second-harmonic band was 250–270 Hz and the sixth-harmonic band was 750–810 Hz.

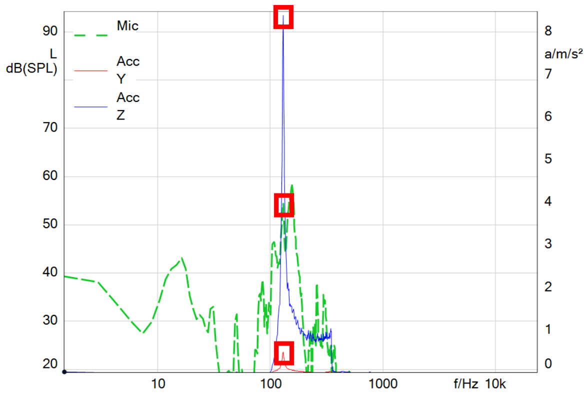

Figure 7: Measured response under 100–350 Hz narrow-band white-noise excitation, confirming the dominant response near 130 Hz in the accelerometer and microphone channels.

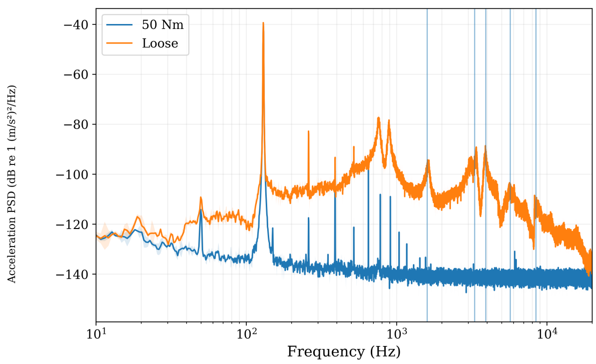

Figure 8: Acceleration PSD for the loose and 50 Nm states under 130 Hz single-tone excitation. Vertical markers identify the five selected loose-state spectral components. PSD levels are expressed in dB relative to $1\,(\mathrm{m/s^2})^2/\mathrm{Hz}$.

As shown in Table 1, the loose state was separated from the 80% state by 17.5 dB in the second-harmonic band and 36.5 dB in the sixth-harmonic band. The repeatability bands of 0.0–0.8 dB were small relative to these differences. The microphone spectra confirmed sound radiation around the selected resonance, but microphone-derived harmonic ratios did not provide a sufficiently repeatable and monotonic separation across all preload states in the present setup; they were therefore not included in Table 1.

The single-tone peaks and the FM harmonic bands are complementary rather than identical features. The selected single-tone components occur at higher-frequency structural response regions and may result from broadband or impact-like energy transfer at the loose interface followed by coupling into structural modes. By contrast, the FM indicators integrate power in predefined bands at integer multiples of the swept carrier. The five single-tone peak frequencies do not coincide with the second- and sixth-harmonic FM bands and were not used to calculate Table 1; both observations nevertheless indicate increased transfer of energy away from the fundamental excitation region when the joint is loose.

Table 1: Mean harmonic-band level relative to the carrier, with ± one standard deviation across three repeated measurements. Values are in dB. Less negative values indicate stronger harmonic-band power relative to the carrier.

Preload	$l=2$	$l=6$
Loose	-43.8 ± 0.4	-21.5 ± 0.4
20%	-55.5 ± 0.1	-53.7 ± 0.6
40%	-58.8 ± 0.0	-53.4 ± 0.8
80%	-61.3 ± 0.1	-58.0 ± 0.5

4. Discussion

The response near 130 Hz provided a reproducible carrier region for comparing preload states. A reduction in preload changes the joint boundary condition from predominantly sticking contact toward partial slip and intermittent contact, which can reduce effective stiffness, increase frictional loss, and strengthen nonlinear energy transfer [12]–[18]. The additional response features observed in the loose state are therefore consistent with known joint-dynamics mechanisms, although the present measurements do not independently separate micro-slip, impacts, and coupling to higher structural modes.

The higher-frequency components in Fig. 8 should not be interpreted automatically as new eigenmodes created by loosening. A more precise interpretation is that they are spectral components that are absent or substantially weaker in the tight-state response. Intermittent contact can generate broadband and harmonic content, which may then excite existing higher-frequency modes of the assembly [12], [15], [18]. This explains why the prominent single-tone components can occur far above exact integer multiples of 130 Hz and why they need not coincide with the harmonic bands used for FM analysis.

The carrier-normalized harmonic-band metric provides a simple measure of nonlinear energy redistribution. The second-harmonic result decreased progressively from the loose state to 20%, 40%, and 80% preload, while the sixth-harmonic band gave the largest loose-to-tight contrast. Higher-order bands are generally more difficult to excite in an approximately linear system, so a strong sixth-harmonic region can be a sensitive indicator of pronounced nonlinearity [12], [18], [35]. However, the small difference between the 20% and 40% sixth-harmonic means shows that the metric should currently be used primarily for separating the fully loose condition from preloaded states, not for estimating preload continuously.

FM excitation offers robustness to small resonance shifts because it repeatedly covers the 125–135 Hz region rather than relying on one exact frequency [20], [22]. It also creates predefined harmonic bands that can be integrated instead of tracking individual narrow peaks. FM does not itself create a loosening signature;

it provides a repeatable way to probe the resonance region and expose differences in nonlinear transfer [35]–[37]. The single-tone test, in contrast, made the broadband elevation and high-frequency components particularly visible. A practical monitoring procedure may therefore use FM band ratios for robust screening and a single-tone spectrum for diagnostic confirmation.

The microphone had a deliberately secondary role. It demonstrated that the selected structural resonance also produced measurable radiated sound and therefore supports the longer-term possibility of non-contact acoustic monitoring. Its weaker preload ordering in the present experiment is plausible because sound radiation depends not only on joint dynamics but also on structural radiation efficiency, sensor distance, room reflections, and background noise [27]–[34]. Future acoustic evaluation should use controlled microphone positions, background-noise characterization, and transfer-function or coherence analysis between acceleration and sound before microphone-only classification is claimed.

The method is most directly applicable to accessible joints during maintenance inspections. Shaker size, reaction-force requirements, and mounting access remain important constraints for bogie-level or densely packaged locations. Compact exciters, impact-based excitation, or operational-response methods should therefore be compared with the present laboratory shaker approach. The current demonstrator also represents only one joint geometry and one varied bolt; transfer to carbody, roof-mounted equipment, bogie assemblies, and bolted elements of rail fastening systems requires validation under representative boundary conditions and environmental variability.

5. Conclusion

Controlled excitation around a dominant 130 Hz response revealed clear differences between loose and preloaded states of the central bolt in a three-bolt lap joint. The accelerometer z-axis showed additional high-frequency spectral components during single-tone excitation, while FM excitation produced carrier-normalized second- and sixth-harmonic band levels that separated the loose and 80% states by 17.5 and 36.5 dB, respectively. The microphone verified acoustic radiation of the target resonance but did not yet provide sufficiently consistent preload ordering for the quantitative metric. The method remains a proof of concept limited to one demonstrator, one varied bolt, discrete torque settings, and three repetitions. Future work should include direct clamp-force measurement, additional geometries and bolts, coherence-based vibro-acoustic analysis, realistic maintenance excitation, and validation on carbody, roof, bogie, and rail-fastening-system joints.

6. Acknowledgements

This work was funded by the European Regional Development Fund (ERDF/EFRE) and the State of Brandenburg within the StaF-Verbund programme, under the project “Systementwicklung für intelligente und automatisierte mobile Inspektion von Schienenfahrzeugen (SIAMIS)”, administered by the Investment Bank of the State of Brandenburg (ILB).

References

[1] National Aeronautics and Space Administration: “Fastener Design Manual,” NASA Reference Publication 1228, 1990.

[2] H. Gong: “Review of research on loosening of threaded fasteners,” *Friction*, vol. 10, no. 3, pp. 335–359, 2022. DOI: 10.1007/s40544-021-0497-1.

[3] Deutsches Institut für Normung: DIN 25201-4:2021-11, “Design guideline for railway vehicles and their components–Bolted joints–Part 4: Securing of bolted joints,” 2021.

[4] G. H. Junker: “New criteria for self-loosening of fasteners under vibration,” SAE Technical Paper 690055, 1969.

[5] Deutsches Institut für Normung: DIN EN 12663-1:2024-02, “Railway applications - Structural requirements of railway vehicle bodies - Part 1: Locomotives and passenger rolling stock (and alternative method for freight wagons),” 2024.

[6] A. Örvnäs: “Methods for Reducing Vertical Carbody Vibrations of a Rail Vehicle - Literature Survey,” KTH Royal Institute of Technology, report, 2010.

[7] A. Mosleh *et al.*: “Recent advances in wayside condition monitoring for railways: a comprehensive review,” *Railway Engineering Science*, 2026. DOI: 10.1007/s40534-025-00423-2.

[8] I. Bravo, U. Alvarado, J. Nieto, and P. Ciaurriz: “Onboard accelerometers in railway track condition monitoring. A systematic review,” *Transportation Research Interdisciplinary Perspectives*, vol. 33, 101572, 2025. DOI: 10.1016/j.trip.2025.101572.

[9] Deutsches Institut für Normung: DIN 65151:2002-08, “Dynamic testing of the locking characteristics of fasteners under transverse loading conditions (vibration test),” 2002.

[10] B. Pichoff: “Bolt self-loosening, an old problem revisited,” *Materiaux & Techniques*, vol. 106, art. 607, 2018. DOI: 10.1051/mattech/2018034.

[11] International Organization for Standardization: ISO 16130:2015, “Aerospace series–Dynamic testing of the locking behaviour of bolted connections under transverse loading conditions (vibration test),” 2015.

[12] Y. Wang *et al.*: “Experimental studies on the energy dissipation of bolted structures with frictional interfaces: A review,” *Friction*, 2024. DOI: 10.1007/s40544-023-0809-8.

[13] D. O. Smallwood: “Damping investigations of a simplified frictional shear joint,” technical report, 2000.

[14] M. Ahmadian and H. Jalali: “Identification of bolted lap joints parameters in assembled structures,” *Mechanical Systems and Signal Processing*, vol. 21, no. 2, pp. 1041–1050, 2007.

[15] N. Jamia, H. Jalali, J. Taghipour, M. I. Friswell, and H. H. Haddad Khodaparast: “An equivalent model of a nonlinear bolted flange joint,” *Mechanical Systems and Signal Processing*, vol. 153, art. 107507, 2021. DOI: 10.1016/j.ymssp.2020.107507.

[16] M. Krack *et al.*: “The Tribomechadynamics Research Challenge: Confronting blind predictions for the linear and nonlinear dynamics of a thin-walled jointed structure with measurement results,” *Mechanical Systems*

and Signal Processing, vol. 224, art. 112016, 2025. DOI: 10.1016/j.ymssp.2024.112016.
[17] A. A. Morsy and P. Tiso: "Predicting the variability of the dynamics of bolted joints using polynomial chaos expansion," *Mechanical Systems and Signal Processing*, 2025.
[18] D. Bograd, P. Reuss, A. Schmidt, L. Gaul, and M. Mayer: "Modeling the dynamics of mechanical joints," *Mechanical Systems and Signal Processing*, pp. 2801–2826, 2011.
[19] N. Li *et al.*: "Monitoring of bolt looseness using piezoelectric transducers: Three-dimensional numerical modeling with experimental verification," *Journal of Intelligent Material Systems and Structures*, 2020. DOI: 10.1177/1045389X20906003.
[20] D. J. Ewins: *Modal Testing: Theory, Practice and Application*, 2nd ed. Baldock, UK: Research Studies Press, 2000.
[21] Brüel & Kjaer: "Mechanical Mobility Measurements," Technical Review BR 0458-012, 2012.
[22] Brüel & Kjaer: "Frequency Response Function Measurements: Shaker Excitation," Application Note BO 0419-11, 2012.
[23] T. Eraliev *et al.*: "Vibration-Based Loosening Detection of a Multi-Bolt Structure Using Machine Learning Algorithms," *Sensors*, vol. 22, no. 3, art. 1210, 2022. DOI: 10.3390/s22031210.
[24] N. Nicholas, J. Wilson, and C. J. Stowell: "Feasibility of using low-sampled accelerometer measurements for bolt joint looseness detection," *IET Renewable Power Generation*, vol. 16, no. 12, pp. 2762–2777, 2022.
[25] I. Ho, A. M. Boor, S. Vanlanduit, and J. V. Dirckx: "Bolt looseness detection using Spectral Kurtosis analysis for structural health monitoring," in *Proc. ISMA/USD*, 2020.
[26] S. M. Sah, J. J. Thomsen, M. Brons, and N. A. Jørgensen: "Estimating bolt tightness using transverse natural frequencies," *Journal of Sound and Vibration*, vol. 431, pp. 137–149, 2018. DOI: 10.1016/j.jsv.2018.05.040.
[27] L.-Y. Hou and D.-B. Zhuo: "Research on bolt loosening recognition based on sound signal and GA-SVM-RFE," *Scientific Reports*, vol. 15, art. 24165, 2025. DOI: 10.1038/s41598-025-08730-8.
[28] L. Cheng *et al.*: "Sound Sensing: Generative and Discriminant Model-Based Approaches to Bolt Loosening Detection," *Sensors*, vol. 24, no. 19, art. 6447, 2024. DOI: 10.3390/s24196447.
[29] Y. Zhou *et al.*: "Percussion-based bolt looseness identification using vibration-guided sound reconstruction," *Structural Control and Health Monitoring*, vol. 29, no. 2, e2876, 2022. DOI: 10.1002/stc.2876.
[30] Y. Zhang *et al.*: "Bolt loosening detection based on audio classification," *Advances in Structural Engineering*, vol. 22, pp. 2882–2891, 2019. DOI: 10.1177/1369433219852565.
[31] F. Wang *et al.*: "Bolt-looseness detection by a new percussion-based method using multifractal analysis and gradient boosting decision tree," *Structural Health Monitoring*, 2020. DOI: 10.1177/1475921720912780.
[32] Z. Yang *et al.*: "Bolt preload monitoring based on percussion sound signal and convolutional neural network (CNN)," *Nondestructive Testing and Evaluation*, 2022. DOI: 10.1080/10589759.2022.2030735.
[33] Z. Jiang *et al.*: "Identification of Bolt Loosening Damage of Steel Truss Structure Based on MFCC-WPES and Optimized Random Forest," *Applied Sciences*, vol. 14, no. 15, art. 6626, 2024. DOI: 10.3390/app14156626.
[34] R. Yuan, Y. Lv, Q. Kong, and G. Song: "Percussion-based bolt looseness monitoring using intrinsic multiscale entropy analysis and BP neural network," *Smart Materials and Structures*, vol. 28, art. 125001, 2019. DOI: 10.1088/1361-665X/ab3b39.
[35] Z. Zhang, M. Liu, Y. Liao, Z. Su, and Y. Xiao: "Contact acoustic nonlinearity (CAN)-based continuous monitoring of bolt loosening: Hybrid use of high-order harmonics and spectral sidebands," *Mechanical Systems and Signal Processing*, vol. 103, pp. 280–294, 2018. DOI: 10.1016/j.ymssp.2017.10.009.
[36] H. Gong, J. Huang, J. Liu, and X. Deng: "Proof-of-concept study of high-order sideband for bolt loosening detection using vibroacoustic modulation method," *Mechanical Systems and Signal Processing*, vol. 169, art. 108638, 2022. DOI: 10.1016/j.ymssp.2021.108638.
[37] N. Zhao, L. Huo, and G. Song: "Vibration acoustic modulation for bolt looseness monitoring based on frequency-swept excitation and bispectrum," *Smart Materials and Structures*, vol. 32, art. 034004, 2023. DOI: 10.1088/1361-665X/acb579.
[38] J. C. Pineda Allen and C. T. Ng: "Nonlinear Guided-Wave Mixing for Condition Monitoring of Bolted Joints," *Sensors*, vol. 21, no. 15, art. 5093, 2021. DOI: 10.3390/s21155093.